2000

Modelling of In-Situ Liquid Chillers

M. W. Browne
The University of Auckland

P. K. Bansal
The University of Auckland

MODELLING OF IN-SITU LIQUID CHILLERS

M.W. Browne and P.K. Bansal
Department of Mechanical Engineering
The University of Auckland, NEW ZEALAND

ABSTRACT

This paper presents an overview of various simulation techniques that may be useful for predicting the in-situ (dynamic) performance of vapour-compression liquid chillers over a wide range of operating conditions. Four models were considered namely steady-state and transient physical models, and steady-state and transient neural network models. Typical real-time operating data taken under various conditions including start-up, quasi-static and modulating operation were used as input to the four models. The predicted performance was then compared to the experimental data to see under what conditions each model may be suitably applied. It was found that steady-state models can give fairly accurate results under quasi-dynamic conditions with the dynamic models performing better under strongly dynamic conditions such as start-up, shutdown, and during sudden changes in load condition.

INTRODUCTION

Vapour-compression liquid chillers are employed to provide chilled water for air-conditioning purposes in commercial and industrial applications. It is a well known fact in the HVAC industry [1-6] that for the majority of the time these machines operate under part-load conditions (away from design conditions) which generally results in reduced coefficient of performance (COP). Computer simulation is therefore an invaluable tool to enable the engineer to predict the performance of a chilling system over a wide range of conditions. It also provides a means of optimising the operation of the system and also with some modification it can be used as a diagnostic tool by comparing actual chiller performance to that of a validated model. However, under in-situ conditions the transient nature of the load presented to the chiller by the building or heat load becomes a major concern to accurate performance prediction. The two main sources of load are people (i.e. building occupancy) and climatic changes which vary over the course of the day and over the space of a year. The effect of these two parameters may also be compounded by the control system for the chiller(s) in a cooling system. For example, a poorly tuned chilled water circuit may cause the chiller to swing drastically from low-to-high loads or cause the chiller to shut-down and start-up frequently. This paper briefly addresses the issue by applying various steady-state and dynamic models to in-situ chiller data of varying dynamic "strengths". Both physical and neural network models are addressed.

CHILLING SYSTEM OVERIVIEW AND EXPERIMENTAL DATA

The models were applied to one twin-screw chillers and one single-screw chiller. These chillers form part of a recently commissioned commercial system that provides chilled water to a network of buildings at the School of Medicine, The University of Auckland, New Zealand. Both chillers have flooded evaporators and water-cooled condensers that are shell-and-tube type (refrigerant on the shell-side) with a single shell pass and two tube passes. The tubes are made of copper whose surfaces have enhanced fins. They modulate their cooling capacity based on the chilled water flow temperature and total load and can operate down to 10% of their rated full load capacity. Typical design conditions are 6°C for the chilled water flow temperature and 29°C for the condenser water inlet temperature. The details of the chillers are summarised in Table 1.

Table 1: Details of the chillers used in validating the steady-state model.

Chiller	Compressor Type	Cooling Capacity (kW)	Refrigerant Type	Evaporator Water Flow Rate (kg/s)	Condenser Water Flow Rate (kg/s)
A	Single-screw	650	HCFC-22	40.6	27
B	Twin-screw	300	HFC-134a	13.7	14.1

The water temperatures (chilled water flow and return, and condenser water flow and return) were measured with T-type thermocouples with an accuracy of ±0.25°C. The mass flow rates were found using a relationship between the water flow rate and the pressure drop across each respective pump. During the gathering of data, an ultrasonic transit time mass flow meter was employed with an accuracy of ±1%. A clamp-on power factor/ampere meter with an accuracy of ±0.5% was employed to determine the compressor electrical work input. Figures 1 and 2 show the typical operation of Chillers A and B under different operating conditions. It can be seen that the operation of the chillers is far from steady state even under quasi-static operation (Figure 1b).

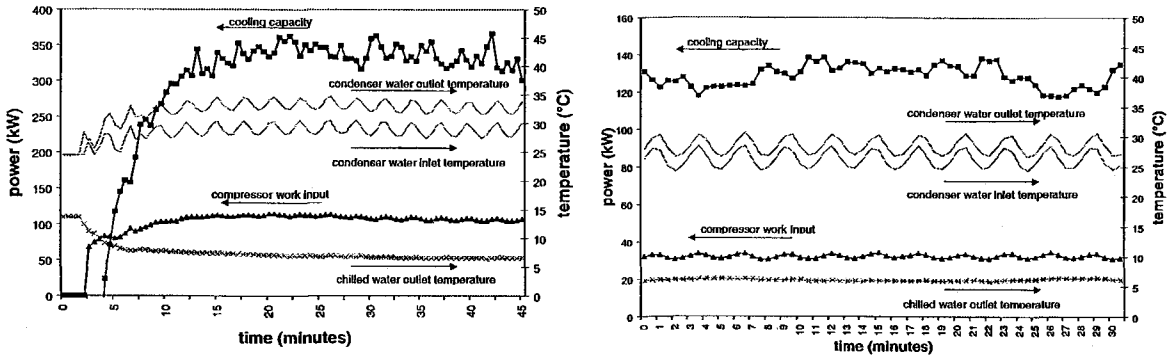

Figure 1: Typical operation of (a) Chiller A during start-up and (b) Chiller B during quasi-static operation.

MODELLING

Four modelling techniques are briefly described in this paper and are used to predict the performance of both chillers under dynamic (in-situ) conditions.

(1) Steady-State Physical Model

Both heat exchangers (evaporator and condenser) are modelled using an elemental NTU-ε method [7]. The basic principle of this approach is to divide both the tube-side region (ie. water) and the shell-side region (ie. refrigerant) into elements to better predict the heat transfer. This requires the length of each tube to be divided into an arbitrary number of elements (of length 'dx') and that the tube bundle be divided into elements dictated by the number of tube rows in the bundle ('dy'). Figure 2 shows a schematic of the methodology for a condenser with "i" elements along the tubes and "j" tube rows. As the water enters the heat exchanger it will either be cooled (as for the evaporator) or heated (as for the condenser). This change in temperature from the entry to the exit of the heat exchanger alters the temperature gradient between the refrigerant and water-sides and hence has a large effect on the heat transfer coefficients. By dividing the heat exchanger into elements, this effect on the heat transfer can be more realistically modelled. Also as the refrigerant enters the tube bank, pressure drops resulting from drag and momentum losses cause the local saturation temperature of the refrigerant to vary throughout the heat exchanger, again affecting the heat transfer coefficients. Once again the row-by-row formulation allows these changes to be accounted for, increasing the realism of the simulation.

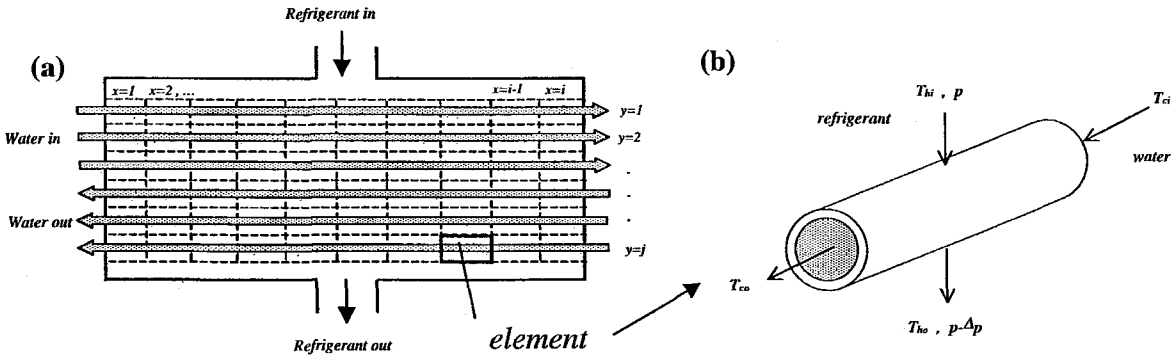

Figure 2: Elemental approach for a shell-and-tube for (a) entire heat exchanger and (b) a single tube element.

The total heat transfer in each was found by summing the heat transfer in all of the individual elements as:

$$\dot{Q}_{total} = \sum_{1}^{a}\sum_{1}^{b}\sum_{1}^{c}\dot{Q}_{act_{abc}} \tag{1}$$

where "a" is the number of passes, "b" the number of rows per pass, and "c" the number of lineal elements in the heat exchanger . The state of the refrigerant was tested in each element to determine whether it was in a single phase condition (as for superheating in the evaporator or desuperheating in the condenser) or a two-phase condition (as in the phase change regions in both heat exchangers). The simple model was used for the compressor where the isentropic efficiency was calculated as a function of refrigerant flow rate and the pressure ratio of the chiller.

(2) Simple Physical Dynamic Model

The main assumptions of the model [8] are:

- The mass flow rate of the refrigerant is assumed to be the same throughout the system.
- The amount of refrigerant in various components neglected.
- The temperature of the walls does not vary through the cross-section or along the length of the tubes.
- Refrigerant properties within each component are homogeneous and pressure drops are neglected.

The dynamic variables (those that enter formulation as a time derivative) are:

- Evaporator tube wall temperature (average)
- Condenser tube wall temperature (average)
- Chilled water temperature (average)
- Condenser water temperature (average)

The modelling of the four dynamic variables are lumped to thermal capacities at their respective temperatures. The drawback of this "thermal" approach is that it cannot tell how well the heat exchangers are utilised in terms of area used for phase transition. Instead it is implicitly described by the parameters of subcooling and superheating. Assuming that the refrigerant is in a quasi-steady state energy balance with the tube wall, the evaporator capacity is given by:

$$\dot{Q}_e = \alpha_{ei} A_{ei}\left(T_{chw} - T_{we}\right) \quad \text{with} \quad \dot{m}_r\left(h_1 - h_6\right) = \alpha_{eo} A_{eo}\left(T_{we} - T_e\right) \tag{2}$$

Similarly for the condenser the capacity is given by:

$$\dot{Q}_c = \alpha_{ci} A_{ci}\left(T_{wc} - T_{cw}\right) \quad \text{with} \quad \dot{m}_r\left(h_2 - h_5\right) = \alpha_{co} A_{co}\left(T_c - T_{wc}\right) \tag{3}$$

Assuming that all of the condenser wall material is at the same temperature the following equations can be derived from the first law of thermodynamics. For the condenser wall temperature during the on and off processes, the rate of change is given respectively by:

$$MC_c \frac{dT_{wc}}{dt} = \alpha_{ci} A_{ci}\left(T_c - T_{wc}\right) - \alpha_{co} A_{co}\left(T_{wc} - T_{cw}\right) \quad \text{and} \quad MC_c \frac{dT_{wc}}{dt} = -\dot{Q}_c \tag{4}$$

Similarly for the evaporator the time derivative for the wall temperature during the on and off processes is given by:

$$MC_e \frac{dT_{we}}{dt} = \alpha_{eo} A_{eo}\left(T_{chw} - T_{we}\right) - \alpha_{ei} A_{ei}\left(T_{we} - T_e\right) \quad \text{and} \quad MC_e \frac{dT_{we}}{dt} = \dot{Q}_e \tag{5}$$

Accounting for the load of the building the following equation can be derived for the time derivative of the chilled water:

$$MC_{chw} \frac{dT_{chw}}{dt} = \dot{Q}_{load} - \dot{Q}_e \tag{6}$$

Similarly for the change in temperature of the condenser water with time the following equation can be derived:

$$MC_{cw}\frac{dT_{cw}}{dt} = \dot{Q}_c - \dot{Q}_{tower} \tag{7}$$

Capacity control is via a slide valve that in turn alters the displacement of the screw compressors based on the chilled water flow temperature and building load. To simulate the control action of the cooling tower an on /off control strategy was employed in an attempt to maintain a set-point (inlet temperature) of 29°C. The appropriate correlations are utilised to calculate the heat transfer coefficients for the condensation [9,10], evaporation [11,12], and the water-side (tube-side) [13]. REFPROP [14] was used to calculate the refrigerant thermophysical properties throughout the cycle.

(3) Steady-State Neural Network Model

The most popular neural networks are the multilayer perceptron (MLP) and the generalised radial basis function (GRBF) network. These networks presently form the basis for the majority of practical applications [15]. In this paper, the GRBF network is chosen [16,17] since it provides several advantages over the MLP network for this application, including fast and efficient training methods, less computationally intensive, and better approximation properties [15]. The diagram shown in Figure 3a can represent the GRBF network. The Gaussian basis functions are situated between the *input* and *output layer* in the *hidden layer*. The architecture of a generalised radial basis function network has c inputs $x_1,...x_c$ and d outputs $y_1,...y_d$. The lines connecting the inputs to the Gaussian function represent (a) the elements of the vector μ_k, which describes the location of the centre (in input space) and (b) the elements of the vector σ_k, which describes the standard deviation of the Gaussian function (in input space). The lines connecting the Gaussian functions to the outputs represent the weights w of the neural network which are comparable to the parameters in the case of curve fitting with simple polynomials. The outputs are then given as a linear combination of the values of the Gaussian functions (see Equation 10). For the general N-dimensional case the k^{th} Gaussian function is given as:

$$G_k(\mathbf{x}) = \exp\left[-\frac{1}{2}\left((\mathbf{x}-\mu_k)^T \sum_k^{-1}(\mathbf{x}-\mu_k)\right)\right], \tag{8}$$

The symbol $\sum_k^{-1}$ is the symmetric $N \times N$ covariance matrix of the k^{th} basis function and represents the standard deviation:

$$\sum_k^{-1} = \begin{bmatrix} \frac{1}{\sigma_{1k}^2} & \cdots & 0 \\ \vdots & \ddots & \vdots \\ 0 & \cdots & \frac{1}{\sigma_{Nk}^2} \end{bmatrix} \tag{9}$$

The basis function parameters ie. the location of the centres and their number, and the standard deviation, are processed in the *hidden layer training*. The output is given as a linear superposition of basis functions, in the form

$$y(\mathbf{x}) = \sum_{k=1}^{ce} G_k(\mathbf{x}) \cdot \mathbf{w}_k \cdot \tag{10}$$

The weights in the vector **w** are subsequently determined in the *output layer training* after the basis function parameters are chosen with use of the sum-of-least squares error function. This error function can generally be written in matrix notation as follows:

$$\mathrm{E} = \frac{1}{2}\left(\mathbf{G}\cdot\mathbf{w}^T - \mathbf{T}\right)^2 \tag{11}$$

where matrix **G** represents all basis functions $G_k(x)$, vector w all weights w_k, and the matrix **T** represents all target values (e.g. the measured data patterns). The error function is minimised when the derivative equals zero which has a unique solution for the weights given by

$$\mathbf{w}^T = \left(\left(\mathbf{G}^T\mathbf{G}\right)^{-1}\mathbf{G}^T\right)\mathbf{T} = \mathbf{G}^{-1}\mathbf{T} \tag{12}$$

(4) Dynamic Neural Network Model

One of the main issues of nonlinear dynamic system identification is the characterisation of the investigated system. The following problem formulation was considered:

$$y(t+1) = f\{y(t), y(t-1),..., y(t-p); u(t), u(t-1),..., u(t-q)\} \tag{13}$$

where $y(t) = [y_1(t), y_2(t)..y_d(t)]$ and $u(t) = [u_1(t), u_2(t)..u_c(t)]$

denote the output vector of the system at time k and the input vector of the system at time t respectively (f is a nonlinear function - see Figure 3b). The dynamic system as given in Equation (12) is then defined by the function f and the integers p and q. If p and q are given, the identification of the model requires finding a suitable function f. Hence the identification procedure consists of adjusting the parameters of the neural network to optimise a performance function based on the error between the plant and the identification model outputs. The two most common identification procedures are the parallel identification structure and series-parallel identification structure In both structures, the network and the system are receiving the same external inputs. In case of the series-parallel identification structure, the network receives feedback from the outputs of the system as part of its input vector. For the parallel structure, the system and the neural network are two independent processes, as the outputs of the system are not used as inputs to the network. For the purpose of this investigation [18] a generalised radial basis function (GRBF) neural network [16,19] and the series-parallel identification structure were used.

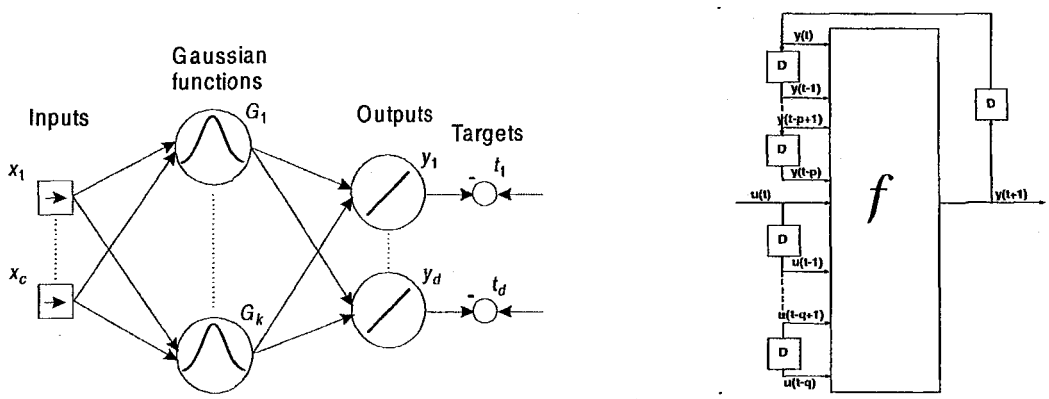

Figure 3: Schematics for the (a) steady-state and (b) dynamic neural network models.

ASSORTED RESULTS

The above models were used to predict the performance of chillers under various modes of dynamic operation including quasi-steady, modulating, and start-up conditions.

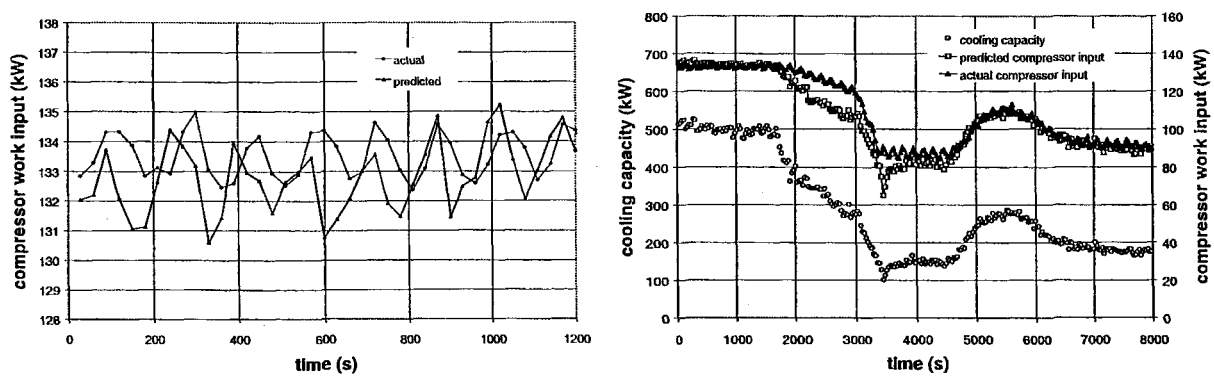

Figure 4: Results for the steady-state physical model (1) for Chiller A for (a) quasi-static operation and (b) varying part-load conditions.

Figure 4 shows results for the steady-state physical model for Chiller A. It can be seen that the agreement during quasi-static operation is excellent with the model predicting values of the compressor work input to within ±5%. However under more dynamic conditions (a decrease in capacity) the predictions are not quite as good with errors of up to 20%. Figure 5 shows some results for the steady-state neural network model. Again while the model gives good results during quasi-static operation it fairs much worse during more dynamic conditions. In this case during increased loading it also has errors of up to 20%. It should be noted that the model can give slightly better results under these more dynamic conditions although the penalty was found to be a lesser accuracy under quasi-static conditions.

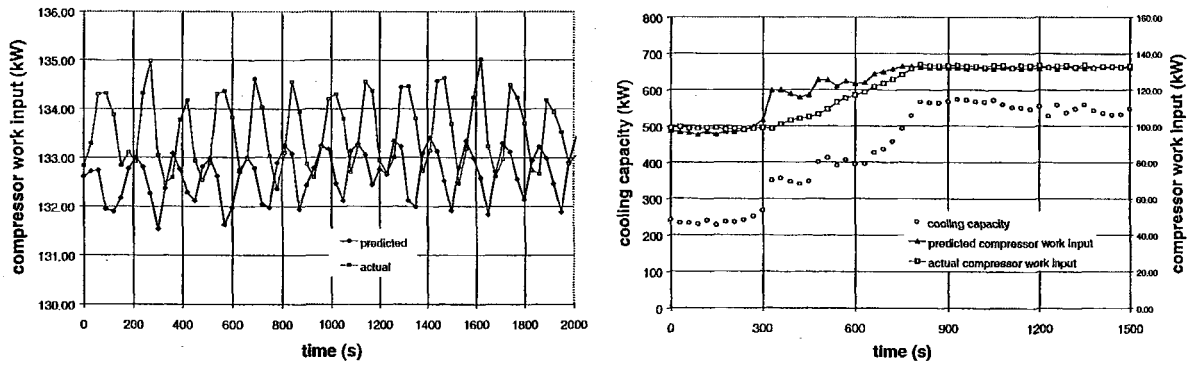

Figure 5: Results for the steady-state neural network model (3) for (a) Chiller A quasi-static operation and (b) Chiller A during an increase in cooling capacity.

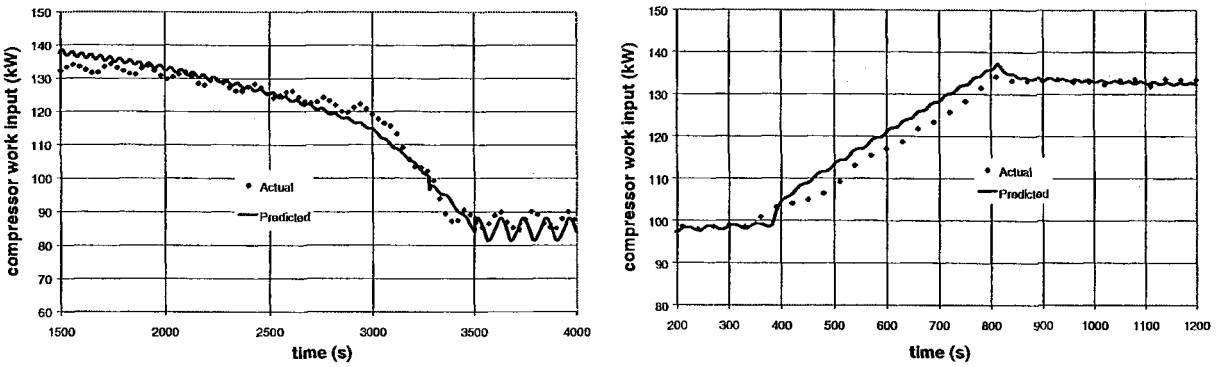

Figure 6: Results for the dynamic model (2) when applied to (a) the decreasing load data from Figure 4 and (b) the increasing load data from Figure 5.

Figures 6a and 6b show the results for the dynamic model when applied to the same dynamic data as the physical steady-state model (Figure 4b) and the neural network steady-state model (Figure 5b) respectively. In both cases the load increase and decrease was represented by a ramp function over the desired period. It can be seen that while the simple dynamic model still has discrepancies it gives better results than both steady-state models with errors being less than 10%.

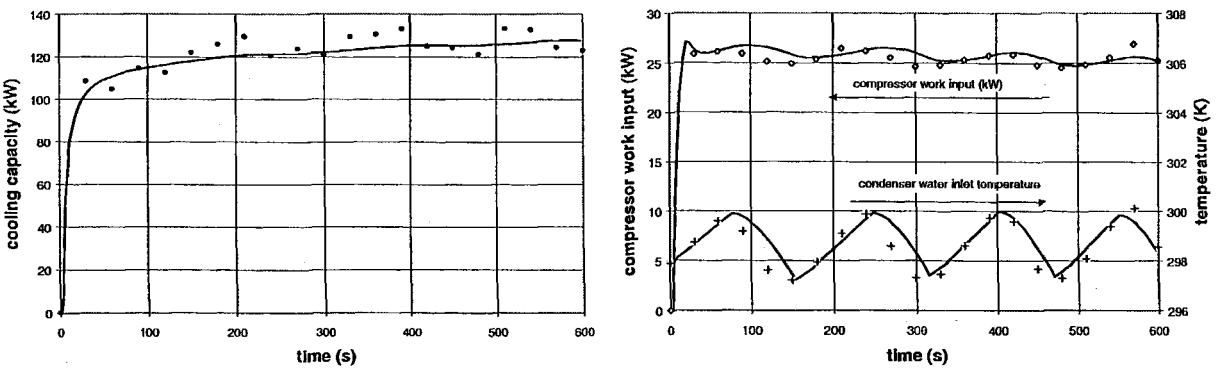

Figure 7: Results for the physical dynamic model for Chiller B under (a) start-up and (b) on/off conditions.

Figure 7 shows the results for the simple physical dynamic model for Chiller B during start-up. It can be seen that even this minimalist approach can provide decent results given known initial conditions. With the addition of more complexity and tuning better results can be expected. Figure 8 shows some results for the dynamic neural network model under different transient conditions. It predicted the majority of values for the compressor work input to within ±5% for Chiller A during start-up and Chiller B during a part-load modulation. As the input data for the model was sampled at 30 second intervals some very steep changes in the function occur. Hence better results can be expected when training and testing the model with experimental data that have been sampled at more frequent intervals. Both the physical and neural network steady-state models require inputs such as the cooling capacity, condenser water inlet temperature, and chilled water outlet temperature at each time step. However, this is not the case with the dynamic models. The neural network models have the disadvantage of being applicable only to the chilling system from which they were derived and also that they are limited to the accuracy of the data that was used to develop them. Outwardly these results look reasonably good. However this study does neglect the internal (ie. refrigerant) state of the chiller. This is something that needs to be addressed in the future.

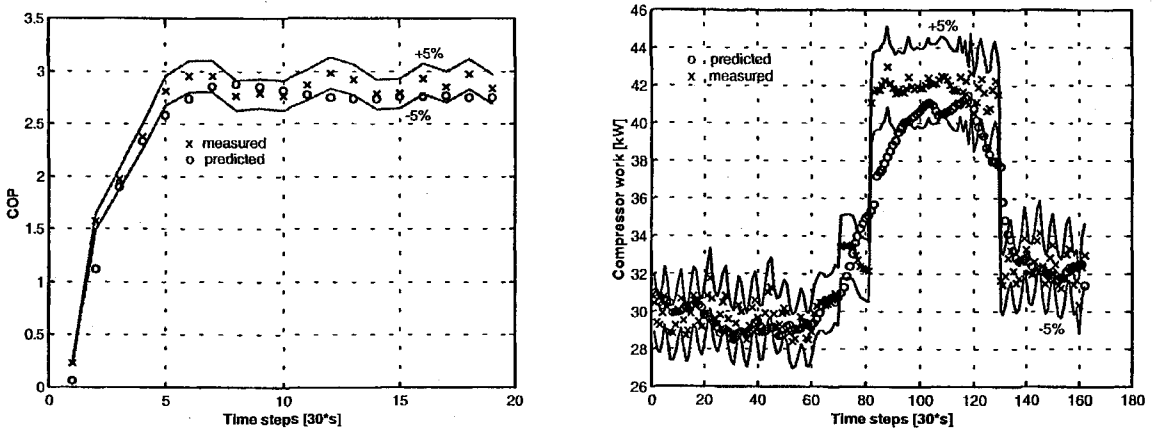

Figure 8: Results for the dynamic neural network model under (a) Chiller A start-up and (b) Chiller B modulating conditions.

CONCLUSIONS

This paper presents a brief overview of the application of various modelling techniques to predict the in-situ performance of liquid chilling systems. It was found that the steady-state models can give excellent results (to within ±5%) during quasi-static operation. However under more dynamic conditions discrepancies of up to ±20% can occur. They also have the obvious limitations during the shutdown process where they will either drastically overestimate the work input or underpredict the cooling capacity depending on the choice of the convergence variable. For those conditions with stronger dynamics the transient models give a better representation of actual performance and in this study predicted the majority of data points to within ±5%. More complex physical dynamic models have been developed and should give a more accurate representation of actual chiller performance.

NOMENCLATURE

A	Area	(m^2)	M	Mass	(kg)
c	Number of neural network inputs		N	Dimension of neural network	
COP	Coefficient of performance		p	Number of aggregates of the output signal	
C	Specific heat	(kJ/kg.K)	q	Number of aggregates of the input signal	
d	Number of neural network outputs		$\dot{Q}$	Heat transfer rate	(W)
G	Gaussian function		y	Neural network output	
$\boldsymbol{G}$	Gaussian values matrix		$\boldsymbol{w}$	Neural network weights vector	
$\boldsymbol{x}$	Input vector		t	Time	
h	Enthalpy	(kJ/kg)	$\boldsymbol{T}$	Target neural network output matrix	
k	k^{th} basis function		T	Temperature	(K)
$\dot{m}$	Mass flow rate	(kg/s)	V_s	Swept volume	(m^3)

$\dot{W}$	Rate of work input/output	(W)

Greek

ε	Heat exchanger effectiveness	
η	Efficiency	
α	Heat transfer coefficient	($W/m^2.K$)
μ	Gaussians center location matrix	
σ	Gaussians standard deviation matrix	

Subscripts

1	Evaporator outlet / compressor inlet
2	Compressor outlet / condenser inlet
3	Saturated vapour condition in condenser
4	Saturated liquid condition in condenser
5	Condenser outlet / expansion valve inlet
6	Expansion valve exit / evaporator inlet
7	Saturated vapour condition in evaporator
chw	Evaporator coolant water
c	Condenser
cw	Condenser coolant water
e	Evaporator
i	Inside
load	Building Load
o	Outside
r	Refrigerant
tower	Cooling tower
wc	Condenser tube wall
we	Evaporator tube wall

REFERENCES

1. **Browne M.W., Bansal P.K.** Challenges in Modelling Vapour-Compression Chillers *ASHRAE Transactions* (1998) **104** (1) Paper no. 4141
2. **Ng K.C., Bong T.Y., Chua H.T.** Performance Evaluation of Centrifugal Chillers in an Air-conditioning Plant With the Building Automation System (BAS) *Proc. Inst Mech Engrs* (1994) **209** 249-255
3. **Beyene A., Guven H., Jawdat Z., Lowrey P.** Conventional Chiller Performances Simulation and Field Data *International Journal of Energy Research* (1994) **18** 391-399
4. **Austin S.B.,** Chilled Water System Optimisation *ASHRAE Journal* (1993) **35** (7) pp 50-56
5. **Bansal P.K., Jager C.R.** Performance Monitoring of Centrifugal *Chillers Proceedings of the Australian Inst. Ref. Aircond and Heating Conference* (1995) 10.
6. **Browne M.W., Bansal P.K.** Steady State Model of Centrifugal Liquid Chillers *International Journal of Refrigeration* (1998) **21** (5) 343-358
7. **Browne M.W, Bansal P.K.,** An Elemental NTU-ε Model for Vapour-Compression Liquid Chillers *Int. J. Refrigeration* (in press 2000).
8. **Browne M.W., Bansal P.K.,** Transient Simulation Model for Vapour-Compression Liquid (submitted 2000).
9. **Beatty K.O., Katz D.L.** Condensation of Vapours on the Outside of Finned Tube *Chemical Engineering Progress* (1948) **44** (1) 55-70
10. **Cavilinni A, Doretti L, Longo G.A, Rossetto L,** A New Model for Forced-Convection Condensation on Integral-Fin Tubes *Journal of Heat Transfer* (1996) **118** pp 689-693
11. **Chen J.C,** Correlation for Boiling Heat Transfer to Saturated Fluids in Convective Flow, Industrial Engineering and Chemical Process Design and Development, Vol. 5, No. 3 (1966), PP 322-329
12. **Webb R.L., Gupte N.S.** A Critical Review of Correlations for Convective Vaporisation in Tubes and Tube Banks *Heat Transfer Engineering* (1992) **13** (3) 58-81
13. **Mills A.F.** Heat Transfer *Richard D. Irwin Inc.* (1992).
14. **Gallagher J., McLinden M., Morrison G., Huber M.** NIST Thermodynamic Properties of Refrigerant Mixtures Database (REFPROP) ver 4.01. *National Institute of Standards and Technology* Gaithersburg USA (1993)
15. **Bishop C.M,** Neural Networks and Their Applications *Rev. Sci. Instrum.* (1994) **65** (6) pp 1803-1832
16. **Swider D.J.,** Experimental Investigation and Neural Network Modelling of Vapour-Compression Liquid Chillers *Student Research Project / Studienarbeit* (1999) University of Auckland, New Zealand
17. **Swider D.J., Browne M.W., Bansal P.K., Kecman V.,** Modelling of Vapour-Compression Liquid Chillers with Neural Networks *Applied Thermal Engineering* (in press 2000).
18. **Bechtler H., Browne M.W., Bansal P.K., Kecman V,** New Approach to Dynamic Modelling of Vapour-Compression Liquid Chillers: Artificial Neural Networks *Applied Thermal Engineering* (submitted 2000).
19. **Chen J.S., Billings S.A.,** Neural Networks for Non-linear System Modelling and Identification *International Journal of Control* (1992) **56** (2), pp 319-346